JOURNAL OF APPLIED ELECTROCHEMISTRY 6 (1976) 431–444

Effects of charge rate and cycling on the morphology of Cd and $Cd(OH)_2$ in sintered plate electrodes

R. BARNARD, G. S. EDWARDS, J. A. LEE, F. L. TYE

Ever Ready Co. (Holdings) Ltd., Central Laboratories, St. Ann's Road, London N15 3TJ

Received 14 November 1975

Optical and scanning electron microscopy have been used to study the growth and redistribution of Cd and $Cd(OH)_2$ in sintered plate electrodes as a function of charge rate and cycle number. As expected, the growth of both components was found to increase with increasing cycle number and decreasing charge rate. Because the deposits, particularly after extended cycling, always contained appreciable quantities of Cd metal in both the charged and discharged state, the sizes of $Cd(OH)_2$ crystallites were difficult to quantify. High charge and discharge rates promoted greater aggregation and redistribution of active material towards the electrode edge. This resulted in a considerable decrease in the available pore volume per unit mass of active material and in extreme cases to localized pore blockage. The trapping of Cd metal by highly crystalline, unchargeable hexagonal platelets of β-$Cd(OH)_2$ resulted in about 50% of the active material becoming obsolete after 100 cycles at high charge and discharge rates. At this stage only the finely divided Cd metal in the electrode interior continued to function. Low charge rates gave deposits of more uniform size and distribution but these contained a high percentage of large Cd particles which discharged less efficiently than those produced at the high charge rate.

1. Introduction

In this communication a detailed study is presented of the relative growth of Cd and $Cd(OH)_2$ in sintered plate electrodes in both the charged and discharged state after cycling under flooded-electrolyte conditions. Both optical and scanning electron microscopy have been employed. Until recently [1] studies of this kind [2] have been made largely on extensively cycled plates removed from commerical cells. Most of these were concerned with the growth of $Cd(OH)_2$ and few have observed the growth of the initially finely divided Cd metal. In this study particular emphasis has been placed on the effects of charge rate on the early cycle behaviour.

Voltammetric [1] and impedance [3] studies have indicated that the Cd particle size increased during cycling particularly at low charge rates. Chemical analysis [1, 4] revealed that in general the discharge process was least efficient. However, at low rates of charge and discharge [4] (long cycle times), charging inefficiencies could also be considerable.

Previous investigations have also recorded that the fall in capacity of the sintered plate electrode during cycling is related to growth of both Cd and $Cd(OH)_2$ [2, 5–7] and to redistribution [8, 9] of the active material. Electrode failure mechanisms based on the restricted diffusion of solution species and pore blocking [10–14] are reported. Armstrong *et al.* [15] attribute failure to the solid-state growth of a passive $Cd(OH)_2$ film beneath the precipitated anodic products.

Comparatively few studies have been made to determine the charging mode of $Cd(OH)_2$. In the case of a planar electrode Okinaka [16] suggests that charging starts by way of a solid-state process with contributions from solution species assuming greater importance towards the end of the process. Several other groups of workers have reached similar conclusions [17–19]. Russian investigations [20, 21] have shown that the efficiency of the charging process involving solution species depends largely on the rate of dissolution of the $Cd(OH)_2$. Chronoamperometry revealed the coexistence of both 'active' and 'inactive' forms of $Cd(OH)_2$, the active form charging at a rate about an order of

magnitude greater than the 'inactive' form. Appelt [22] has demonstrated that the charging efficiency is related to chemical precipitation conditions and that decreasing charge acceptance is caused by progressive formation of a more ordered, sheet-structured, form of β-$Cd(OH)_2$.

Cycling voltametric studies using planar electrodes have repeatedly shown [1, 4, 23] that the anodic products are difficult to reduce completely. Will and Hess [19] using a single simulated pore (essentially a planar electrode) observed the presence of large ($\sim$3 μm) $Cd(OH)_2$ crystals after the 1st cycle discharge which did not reduce on the subsequent charge cycle and concluded that these were the major cause of charge inefficiency. In contrast sintered plate electrodes have been shown [1, 4] to charge relatively efficiently ($\sim$90%) during the early cycles in flooded-electrolyte conditions. Although optical and scanning electron microscopy [5, 7, 24] have clearly shown the presence of large β-$Cd(OH)_2$ crystals in sintered plate electrodes these are generally only seen after extended (>500 cycles) battery cycling. It is interesting to note that Luksha *etal.* [7] could find no correlation between $Cd(OH)_2$ crystallite size and loss in cycling efficiency. Okinaka and Whitehurst [2, 4] demonstrated that hexagonal β-$Cd(OH)_2$ produced at room temperature, having a relatively large crystallite size, charged inefficiently (presumably via soluble species) at low temperatures. The acicular, γ-$Cd(OH)_2$ (stabilized at low temperatures) has been shown to charge more readily both at normal and low temperatures [24].

2. Experimental

2.1. *Sample preparation*

The test electrodes consisted of 1 cm x 1 cm x 0·065 cm samples of nickel sinter impregnated with $Cd(OH)_2$ (0·096 g). Electrodes were charged and discharged under flooded electrolyte conditions in 30% KOH using the test cells and automatic cycling equipment described previously [1]. The charge and discharge cut-off levels were fixed as before at -1050 and -200 mV w.r.t. Hg/HgO/30% KOH at 25°C. All test electrodes were subjected to a formation treatment prior to cycling, namely charging at the $C/2$ rate (18·1 mA) for 16 h.

After the requisite number of cycles had been completed the electrodes in the charged or discharged state were washed thoroughly with water and ethanol both pre-saturated with nitrogen. The samples were dried under vacuum in the port of an evacuable glove-box (Mecaplex G-B3011), after which the samples were cast in epoxy-resin under nitrogen in the main chamber of the glove box.

The electrodes were cut at right angles to the central support strip and the sections abraded using P400 and P600 grade SiC. Polishing was continued using the progression of diamond pastes, 6/14, 1/$\frac{1}{4}$ and $\frac{1}{4}$ μm (Dialap compound and lubricant) and established metallurgical procedures. The final samples were optically flat and scratch-free when viewed at x 1000.

Polishing was initially conducted inside the glove box to minimize oxidation of the finely divided Cd metal in the electrodes. However, it was subsequently found that the samples once cast in epoxy-resin were stable in air for 24 h before a thin oxide film was produced on the surface. Consequently polishing could be carried out more conveniently in air using normal procedures. Samples were finally washed for 30 s in an ultrasonic cleaner tank containing trichloroethylene.

2.2. *Microscopy*

Optical micrographs were obtained using a Vickers-Cooke M55 projection microscope at magnifications up to x 1000.

Scanning electron micrographs were obtained using a Cambridge Scientific Instruments Ltd., 'Stereoscan II A' in conjunction with an Ortec, non-dispersive electron probe microanalyser. Electrode samples containing predominantly Cd metal were sufficiently electrically conducting so that no electrostatic charging of the sample by the electron beam was experienced. On the other hand samples containing large quantities of insulating $Cd(OH)_2$ could be observed directly only at low magnification because of charging effects. Image distortion due to electrostatic charging was eliminated by coating the samples first with a thin layer of carbon and then aluminium (total thickness $\sim 100^{\phi}$ Å). This enabled magnifications up to x 10 000 to be obtained. It should be noted that the conducting film gave good resolution of $Cd(OH)_2$ at the expense of slightly inferior resolution of Cd metal. Consequently the Cd metal

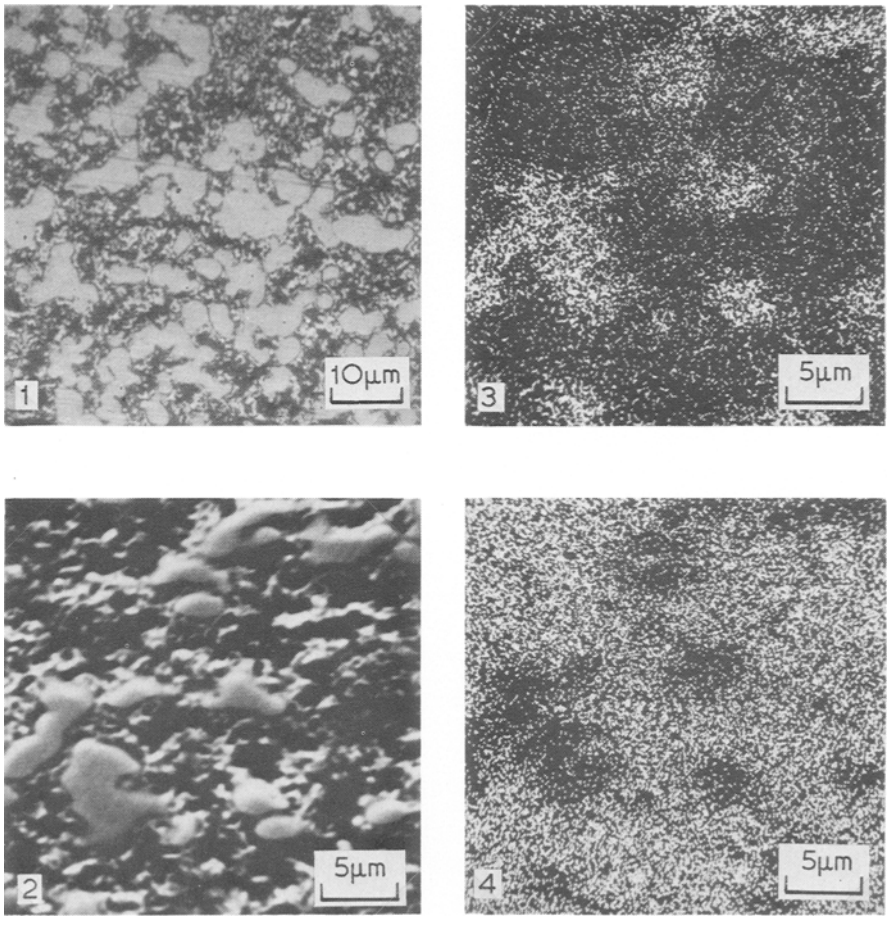

Fig. 1–4. 'Formed' electrode (*C*/2 charge rate for 16 h.). Fig. 1: optical micrograph; Fig. 2: scanning electron micrograph; Fig. 3: Ni distribution in area shown by Fig. 2; Fig. 4: Cd distribution in area shown by Fig. 2.

was studied in detail by SEM and microprobe analysis in uncoated samples only.

3. Results

3.1. *Cadmium metal in charged electrodes*

3.1.1. *'Formed' electrode.* Optical micrographs showing complete sections of cycled and uncycled electrodes at low magnification have been shown previously [1] and will not be duplicated here. Fig. 1 is an optical micrograph of a section of a 'formed' electrode in the charged state. The large white (reflecting) particles are nickel sinter (~5 μm diameter), whilst the much smaller ones (~1 μm diameter) are cadmium metal. The black areas are epoxy-resin. In general the Cd having a slightly whiter contrast could be distinguished by its appearance from the Ni, although, this may not always be clear from the photograph.

To confirm the location of the Cd and Ni particles electron microscopy in conjunction with an electron probe microanalyser was used. As well as spot analyses on specific areas, the analyser enabled distribution maps for individual elements to be obtained. Fig. 2 shows an electron micrograph of the 'formed' electrode. It can be seen that the Cd forms a fine interlocking network within the larger Ni sinter matrix, the average Cd particle diameter is ~0·6 μm. Assuming the particles to be spherical gives a real surface area of ~1·2 $m^2 g^{-1}$. Figs. 3 and 4 give the corresponding elemental distributions of Ni and Cd respectively obtained by the microanalyser. The points of concentration of white dots represent a high probability of finding the specifically programmed element at a

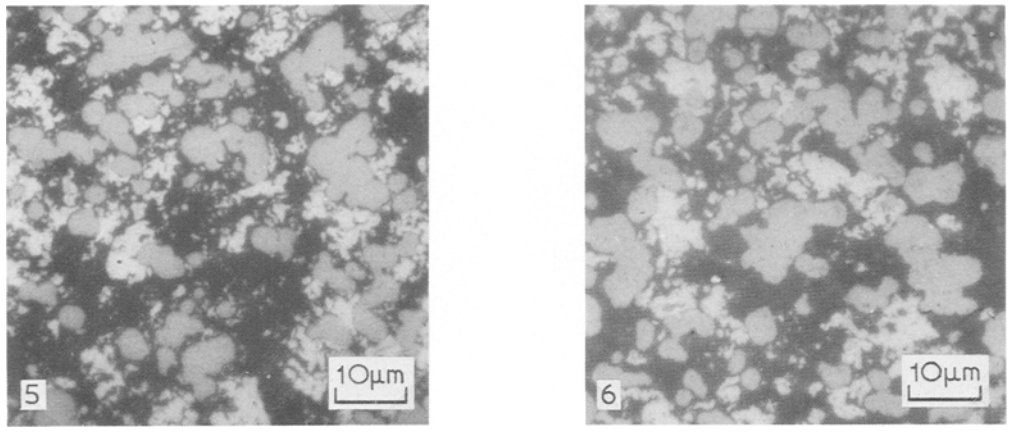

Figs. 5 and 6. Optical micrographs of charged samples cycled at the $C/50$ charge rate, $C/1$ discharge rate regime. Fig. 5: after 2 cycles; Fig. 6: after 6 cycles.

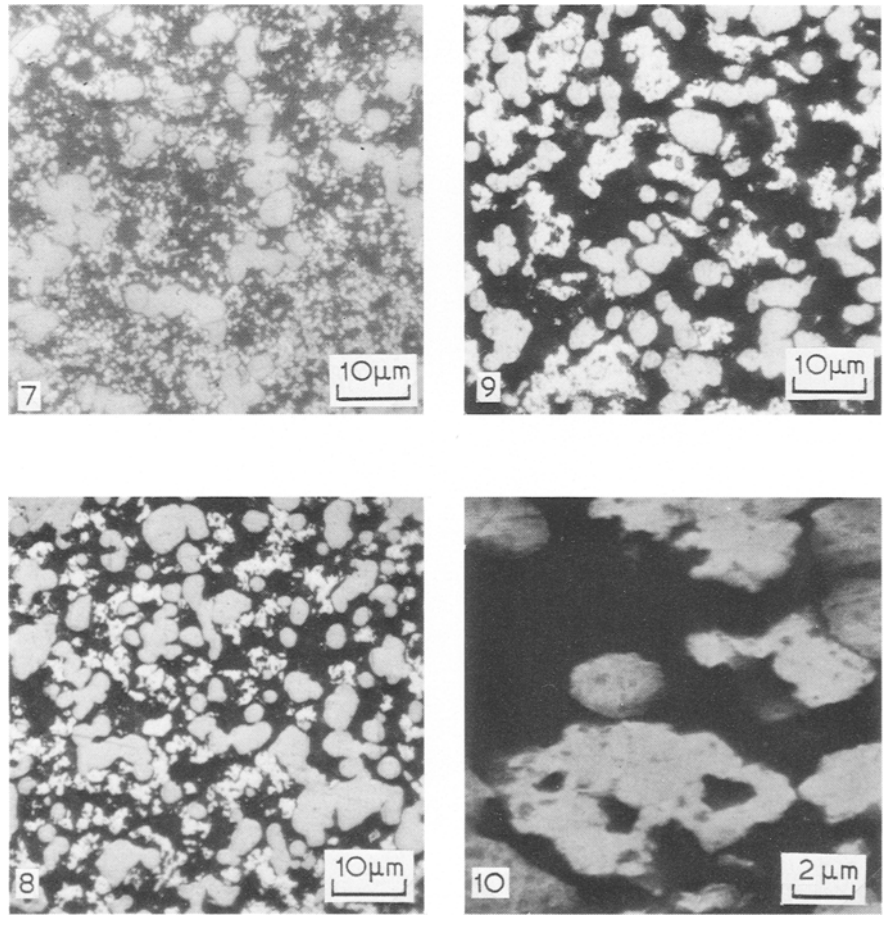

Figs. 7–10. Micrographs of charged samples cycled at the $C/8$ charge rate, $C/1$ discharge rate regime. Fig. 7: after 2 cycles; Fig. 8: after 6 cycles; Fig. 9: after 100 cycles; Fig. 10: Scanning electron micrograph after 30 cycles.

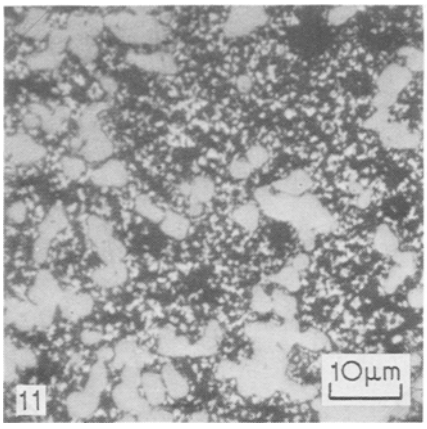

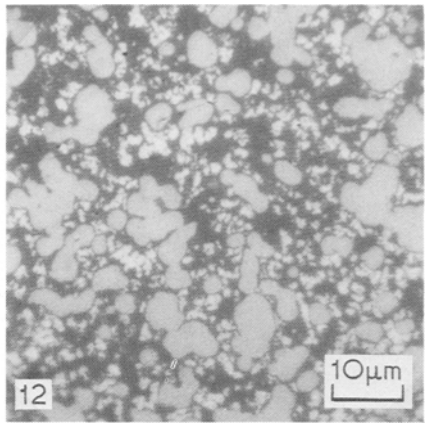

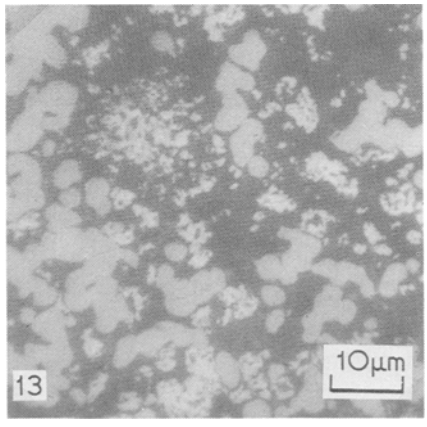

Figs. 11–13. Optical micrographs of charged samples cycled at the $C/1$ charge rate, $C/1$ discharge rate regime. Fig. 11: after 2 cycles; Fig. 12: after 6 cycles; Fig. 13: after 100 cycles.

particular point rather than pin-pointing specific particles. There is inevitably slight overlap observed between the Ni and Cd zones because of scattering effects. Peaks in the X-ray energy spectrum for Ni ($L\alpha$ 0·85 eV, $K\alpha$ 7·50 eV and $K\beta$ 8·24 eV) and Cd ($K\alpha$ 3·13 eV and $K\beta$ 3·31 eV) conclusively identify the elements.

3.1.2. *Cycled electrodes.* Figs. 5 and 6 are micrographs of electrodes, cycled at the $C/50$ charge, $C/1$ discharge rates, removed in the charged state after 2 and 6 cycles. The dramatic increase in Cd particle size is clearly evident. The growth of Cd metal during cycling is also rapid at the $C/8$ charge, $C/1$ discharge rate as seen from Figs. 7–10. Even after only 6 cycles (Fig. 8) the Cd particles are only slightly smaller than the Ni sinter particles. The increase in particle size continues up to 100 cycles (Fig. 9) but the increase from 30 cycles is more gradual than in the early cycles. The compact nature of the Cd particles (lighter contrast) may be judged from the scanning electron micrograph, (Fig. 10), for an electrode in the charged state after 30 cycles. A factor which must be taken into consideration is that because of the growth and build up of unused Cd and $Cd(OH)_2$ during cycling the applied current density is inevitably increasing on each cycle in spite of the galvanostatic conditions employed. This in turn offsets the rate of Cd metal growth and in later cycles an equilibrium state is attained.

Figs. 11–13 are micrographs of electrodes, cycled at the high $C/1$ charge and discharge rates, removed in the charged state after 2,6 and 100 cycles. By comparison with the deposits produced at the $C/8$ and $C/50$ charge rates, these deposits have a more open structure being made up of clusters of small Cd particles having undergone minimal individual growth. Fig. 14 summarizes the average Cd particle size determined from the

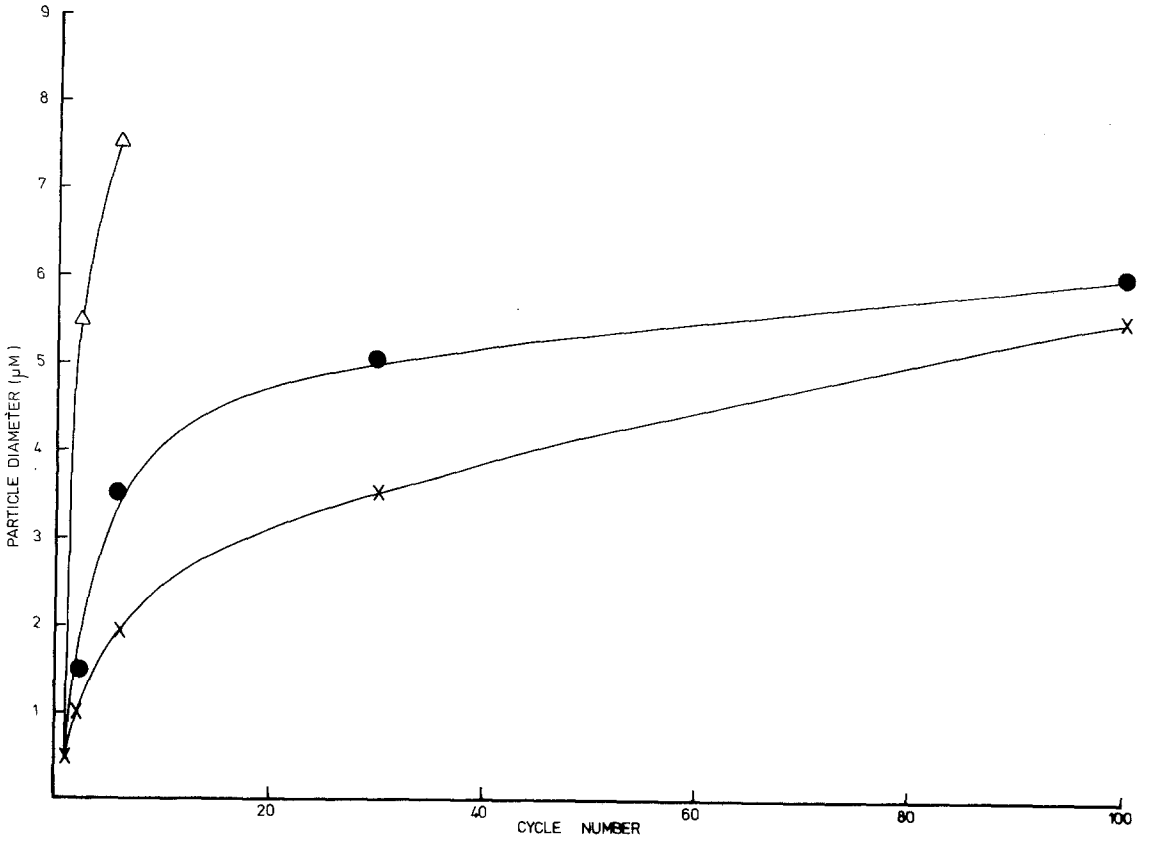

Fig. 14. Cd metal particle diameter as a function of cycle number for charged samples. Discharge rate $C/1$, charge rate: ×, $C/1$; •, $C/8$; △, $C/50$.

photomicrographs as a function of cycle number for the three charge regimes.

The photographs shown so far are for typical central areas within the electrode illustrating the overall progression of Cd growth. However, it should be noted that some gradation of Cd particle size within the electrode is observed during cycling. This effect is not detailed here because of the large number of photographs required. The effect has been briefly illustrated previously at the $C/8$ charge rate [1].

3.2. *Cadmium metal in discharged electrodes*

The presence of undischarged Cd in discharged electrodes after only 6 cycles at the $C/1$ charge and discharge rates can be seen from Fig. 15. Because of its weakly reflecting nature the $Cd(OH)_2$ also present is not well resolved by optical microscopy. It can be just discerned as the dark grey areas surrounding the cores of Cd metal. The hydroxide can be seen clearly by SEM and will be discussed in detail presently. By lowering the charge rate to $C/8$ and $C/50$ the size of the undischarged Cd core in the discharged electrode is much increased as illustrated by Figs. 16 and 17. In general as expected the size of the unused Cd increases with increasing cycle number and decreasing charge rate. These observations correlate with the levels of undischarged Cd determined by chemical analysis [1].

3.3. *Cadmium hydroxide study*

A detailed examination of the $Cd(OH)_2$ present in both charged and discharged electrodes was made using SEM because of the better resolution and higher magnification possible with the technique.

3.3.1. *Discharged electrodes, C/1 rate.* Fig. 18 is a micrograph of the 'formed' electrode after discharge at the $C/1$ rate, obtained by SEM. A mass

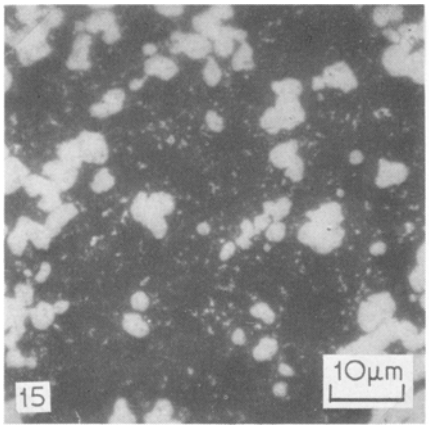

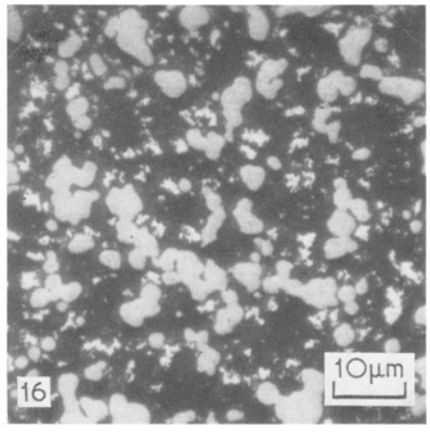

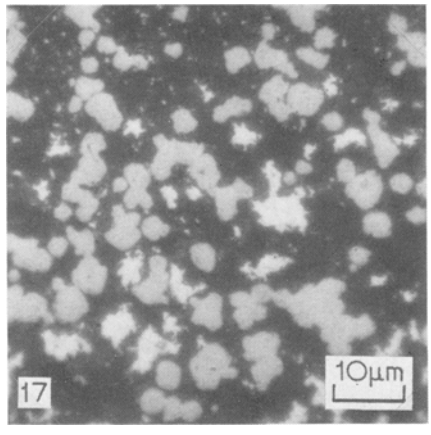

Figs. 15–17. Optical micrographs of discharged samples after 6 cycles. Discharge rate $C/1$, charge rate; Fig. 15: $C/1$; Fig. 16: $C/8$; Fig. 17: $C/50$.

of small $Cd(OH)_2$ particles of ill-defined shape (~1 μm diameter) can be seen between the large sinter particles (~4 μm diameter). Fig. 19 shows a micrograph of an electrode in the discharged state after 6 cycles at the $C/1$ charge and discharge rates. By comparison with Fig. 18 it can be seen that very little individual $Cd(OH)_2$ particle growth has taken place although there is greater aggregation. Undischarged Cd metal can also be seen with difficulty as the whiter patches within the $Cd(OH)_2$ deposits. Its presence can be demonstrated more readily by optical microscopy as seen previously, Fig. 15.

Fig. 20 is a micrograph of a sample in the discharged state after 100 cycles at the $C/1$ charge/discharge regime. Large masses of $Cd(OH)_2$ (~25 μm across) extending ~90 μm in from the electrode edge can be clearly seen even at this low magnification. The particles on the immediate edge and further into the deep interior of the electrode are smaller, being approximately 3 μm diameter. Figs. 21 and 22 at higher magnification reveal that the particles are highly crystalline having definite hexagonal and quadrilateral shapes. It must be remembered that the samples under study have been sectioned and polished and only a two-dimensional effect is given. The crystals are most likely to be in the form of hexagonal platelets, the normal habit of β-$Cd(OH)_2$. This will also be evident later from Fig. 34. The quadrilateral shapes could be the result of sections through hexagonal platelets or less likely acicular crystals (γ-$Cd(OH)_2$).

It is interesting to note that the well-defined $Cd(OH)_2$ crystals occlude large quantities of irregular-shaped, metallic Cd (white patches within the crystals). Photographs obtained for electrodes after 30 cycles are very similar to those after 100 cycles except that the Cd-$Cd(OH)_2$ compacts are slightly less extensive.

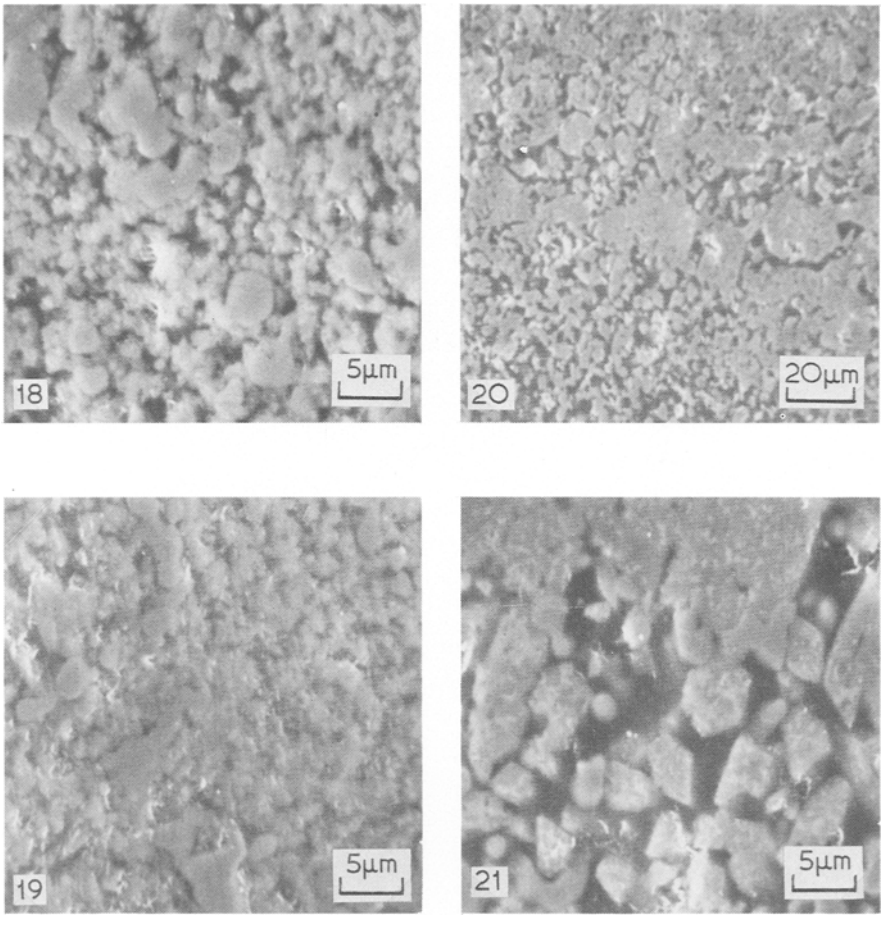

Figs. 18–21. Scanning electron micrographs of discharged samples cycled at the $C/1$ charge rate, $C/1$ discharge rate. Fig. 18: after 1 cycle ('formed' electrode discharged); Fig. 19: after 6 cycles; Fig. 20: after 100 cycles; Fig. 21: as Fig. 20 but at higher magnification.

3.3.2. *Charged state, C/1 rate*. Fig. 23 shows the corresponding micrograph towards the edge of an electrode sample in the charged state after 100 cycles at the $C/1$ charge/discharge regime. It is evident that the large crystalline masses of $Cd(OH)_2$ with occluded Cd are still present after charging. However, further into the electrode, Fig. 24, the particles consist of porous clusters of mainly Cd metal (overall diameter about 4 μm) with individual particles having a diameter of ~0.6 μm. It is likely that the Cd is in a network structure similar to that in the formed electrode. It appears that only Cd in the electrode interior is now participating in the electrode reactions. The large crystalline Cd-$Cd(OH)_2$ masses extending for about 90 μm in from the electrode edge are obsolete. The inability of the large well-defined $Cd(OH)_2$ crystallites to charge also isolates the trapped Cd.

3.3.3. *Discharged state, C/8 charge rate*. Fig. 25 is a micrograph towards one edge of an electrode removed in the discharged state after 6 cycles at the $C/8$ charge, $C/1$ discharge rates. Distinctly crystalline deposits of $Cd(OH)_2$ (~3·5 μm across) may be seen, compared with the lack of definition for the corresponding sample cycled at the $C/1$ charge/discharge rates, Fig. 19. Small particles of Cd (0·6 μm diameter) may be observed within these hydroxide particles. Progressing further into the electrode, Fig. 26 reveals a new zone of particles composed largely of Cd metal (~2·5 μm diameter) encased by a thin layer of $Cd(OH)_2$ about 0·5 μm thick. After 100 cycles at the $C/8$

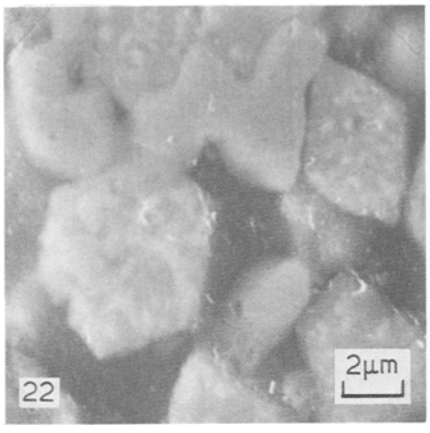

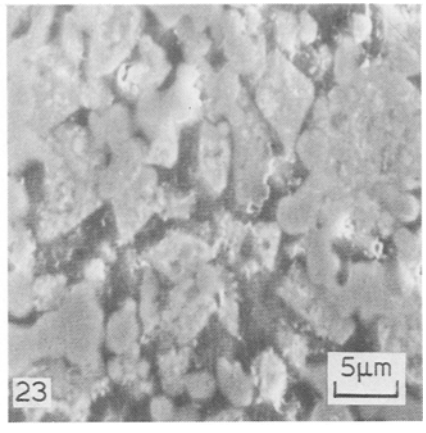

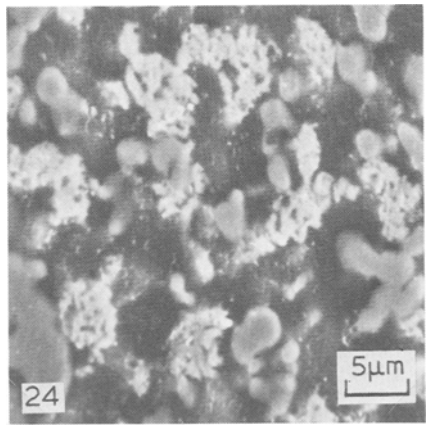

Figs. 22–24. Scanning electron micrographs of samples cycled at the $C/1$ charge rate, $C/1$ discharge rate regime. Fig. 22: discharged sample after 100 cycles (higher magnification of region shown in Fig. 21); Fig. 23: charged sample after 100 cycles, region near electrode edge; Fig. 24: as for Fig. 23 but region in the interior.

charge, $C/1$ discharge rates, Fig. 27, the Cd-$Cd(OH)_2$ deposits are smaller than those produced at the $C/1$ charge regime (Fig. 20). On the very edge of the electrode is a thin layer of predominantly $Cd(OH)_2$ particles (1 μm diameter). Further into the electrode the aggregates of active material are about 5 μm across and have a fairly uniform distribution throughout the remaining electrode. The high degree of crystallinity of the aggregates can be judged from Fig. 28. Although, the deposits produced at the $C/8$ charge rate are smaller in overall size than those at the $C/1$ charge rate, the quantity of Cd (having a greater density) contained within them is larger. Similar behaviour was also observed after 30 cycles.

3.3.4. *Discharged state, C/50 charge rate.* By lowering the charge rate to $C/50$ the onset of greater $Cd(OH)_2$ crystallinity appears after only two cycles as can be seen from Figs. 29 and 30. The predominant factor is however the presence of large cores of unused Cd metal up to 3 μm diameter. This emphasizes the greater inefficiency of the discharge process. Nevertheless, the presence of crystalline $Cd(OH)_2$ at this early stage of cycling is also significant and is the cause of the noticeably lower charge efficiencies previously measured at the $C/50$ rate [1].

Fig. 31 is a micrograph of a discharged electrode after 6 cycles at the $C/50$ charge, $C/1$ discharge rates. Again, extremely large cores of undischarged Cd metal can be clearly seen surrounded by thinner layers of crystallized $Cd(OH)_2$.

Because the growth of $Cd(OH)_2$ is also influenced by the size of the Cd metal deposits, it is difficult to quantify the size of the $Cd(OH)_2$ crystallites as a function of cycle number and charge rate. The obvious difficulty arises from the presence of increasingly large quantities of Cd metal within the apparently unperturbed $Cd(OH)_2$

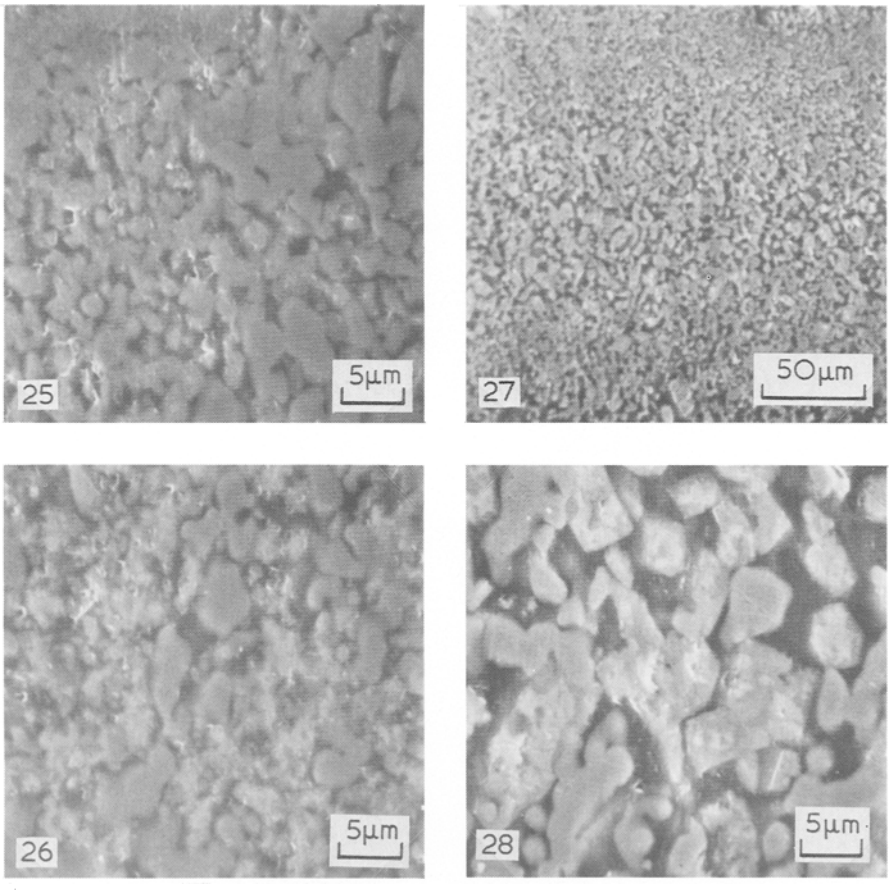

Figs. 25–28. Scanning electron micrographs of discharged samples cycled at the $C/8$ charge rate, $C/1$ discharge rate regime. Fig. 25: after 6 cycles, region near electrode edge; Fig. 26: as for Fig. 25 but region in the interior; Fig. 27: after 100 cycles; Fig. 28: as for Fig. 27 but at higher magnification.

crystals. Nevertheless, an attempt was made to compare the sizes of the particles at various points in the electrode. The results are only very approximate since there is a considerable variation in size and shape of particles within a region and it is also difficult to assess with any certainty the relative proportions of Cd to $Cd(OH)_2$ within a particle. The results are presented in Figs. 32 and 33.

3.4. *Cycled battery plate*

Fig. 34 shows the surface of a negative electrode removed from a commercial cell after several hundred cycles at elevated temperatures. It is clear that the $Cd(OH)_2$ can grow to very large sizes. The hexagonal platelets shown here are ~50 μm from one edge of the hexagon to the other and about 2 μm thick.

4. Discussion

This study vividly demonstrates that during cycling both Cd metal and $Cd(OH)_2$ increase in size particularly at low rates of charge. During the early cycles the growth of large Cd metal particles is an important contributor to capacity loss, confirming previous analytical data [1]. Voltammetric [1] and impedance measurements [3] have similarly detected a drastic fall in working area during cycling for electrodes charged at the $C/8$ and $C/50$ rates. However, after cycling at the $C/1$ rate the measured change in working area was relatively small after 100 cycles in spite of the agglomeration of Cd metal particles shown by Fig. 13. Additionally a fall in Cd area available at all charge rates would be expected [1], irrespective of the Cd particle growth, because of the presence,

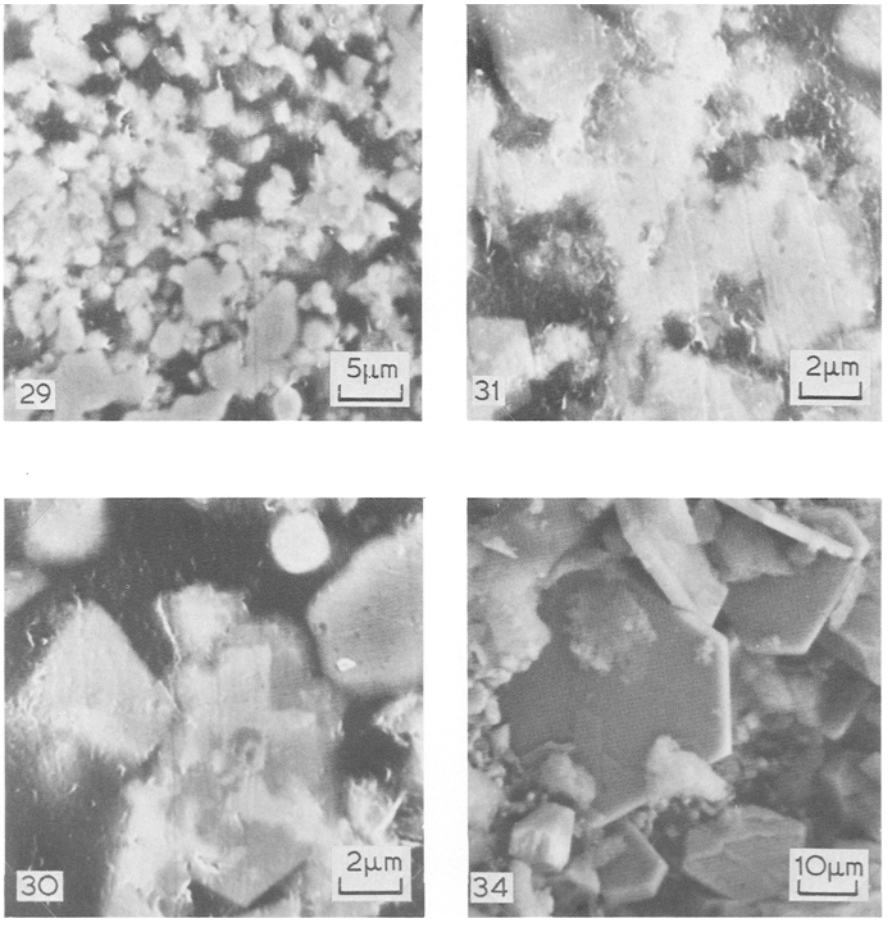

Figs. 29–31. Scanning electron micrographs of discharged samples cycled at the $C/50$ rate, $C/1$ discharge rate regime. Fig. 29: after 2 cycles; Fig. 30: as for Fig. 29 but at higher magnification; Fig. 31: after 6 cycles.

Fig. 34. Scanning electron micrograph of the surface of a discharged battery plate after several hundred cycles at elevated temperatures.

of uncharged $Cd(OH)_2$ after extended cycling reducing the quantity of Cd produced on charge.

The growth of Cd particles at low charge rates is to be expected from electrodeposition theory. High charge rates lead to the formation of a larger number of discrete crystal nuclei whilst low charge rates favour continuous growth on fewer nuclei. It is also energetically more desirable for Cd to deposit on existing Cd sites, thereby completing an unfinished plane in the lattice, rather than to deposit on a dissimilar Ni site.

The observation, that $Cd(OH)_2$ crystals can grow to large dimensions (Fig. 34) on the exterior of heavily cycled battery plates, has led several workers to the conclusion [5, 7, 19, 24] that these are the prime cause of capacity loss during cycling. Because of the growth of large Cd particles particularly at low rates of charge, this is also an important cause of capacity loss during early cycles. Thus superficial examination of the electrode surface can give a misleading impression. Although the overall size of the $Cd(OH)_2$ crystallite after 100 cycles is apparently larger at the high $C/1$ charge rate than at the low $C/8$ charge rate the onset of crystallinity does in fact appear progressively earlier as the charge rate is decreased, i.e. after 2 cycles at the $C/50$ rate, 6 cycles at the $C/8$ rate and ~ 30 cycles at the $C/1$ rate.

The migration and growth of Cd and $Cd(OH)_2$ within the sintered plate electrode point to a substantial involvement of solution species during cycling. Such a process is well-established for

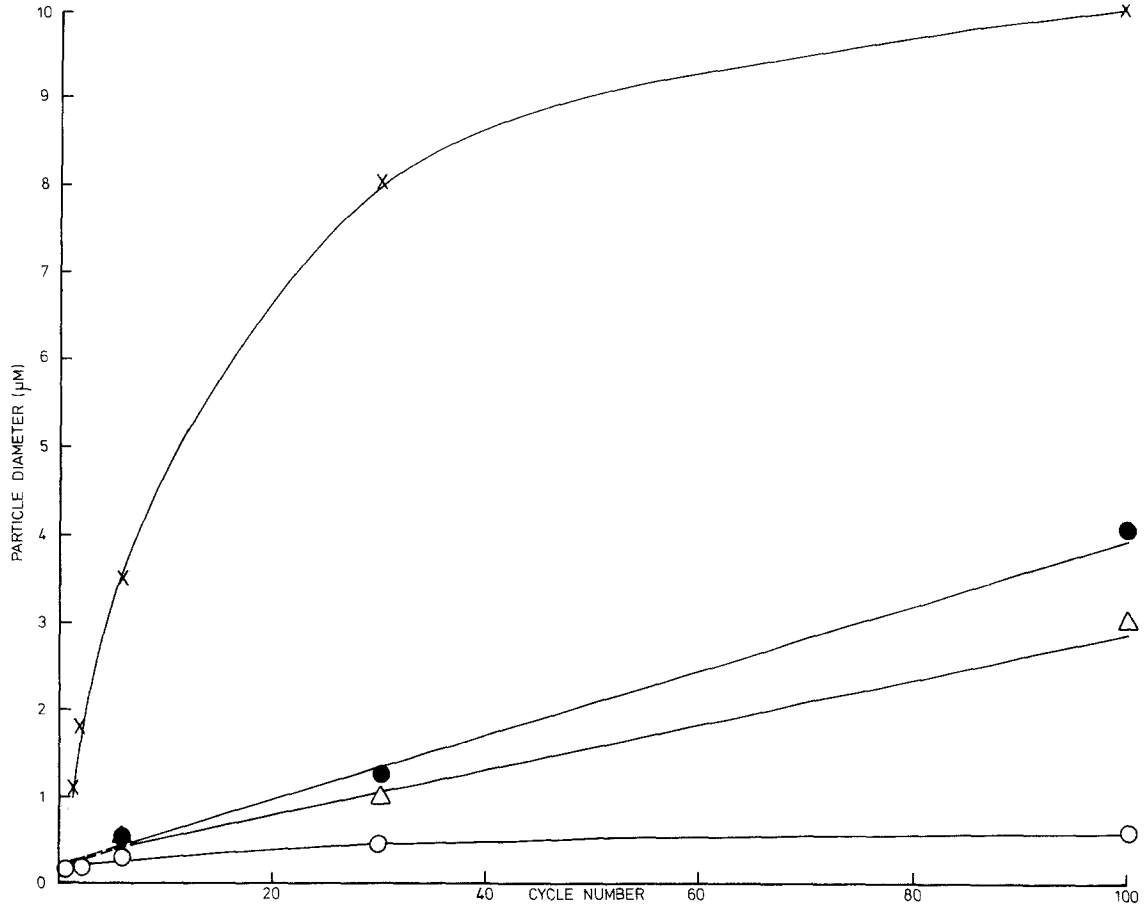

Fig. 32. Particle diameter as a function of cycle number for discharged samples. $C/1$ charge and discharge rates; X, $Cd/Cd(OH)_2$ compacts in electrode edge; ○, trapped Cd in electrode edge; ●, $Cd/Cd(OH)_2$ compacts in electrode interior; △, trapped Cd in electrode interior.

discharge whereas it has only recently been recognized that the majority of charge accepted stems from a soluble entity [25]. Non-uniform redistribution of active material within the electrodes appears to be greatest at the high charge rate ($C/1$), which also facilitates maintenance of small Cd particles. According to Will [26] migration of active material is dependent on pH gradients in the electrode established during charging and discharging. The pH gradients set up local concentration cells which in turn induce current flow between different areas within the electrode [26]. Low charge rates producing a more uniform current distribution would therefore be expected to result in a more uniform distribution of active material. Unfortunately low charge rates also favour the growth of large Cd metal particles and ageing of precipitated $Cd(OH)_2$ also occurs because of the long cycle time involved.

Two different kinds of coverage of Cd metal by $Cd(OH)_2$ can be clearly distinguished after discharge. The first involves a large Cd core surrounded by a thin (~0·5 μm) poorly crystalline coating of $Cd(OH)_2$ (see for example Fig. 31) where the Cd could be considered as rendered inactive either by surface blockage or by an underlying passive film as previously suggested [1]. It is interesting to note that the hydroxide coating observed here is about the same thickness as that estimated (0·4 μm) for the passive film on planar cadmium [27]. Because some cadmium particles continue to increase in size during cycling their $Cd(OH)_2$ layers must still be active.

The second type of deposit involves a smaller Cd core surrounded by a thick highly crystalline layer of $Cd(OH)_2$ (e.g. Fig. 22). The latter is inactive because similar deposits persist after cycling. The inability of the large $Cd(OH)_2$ crystals to

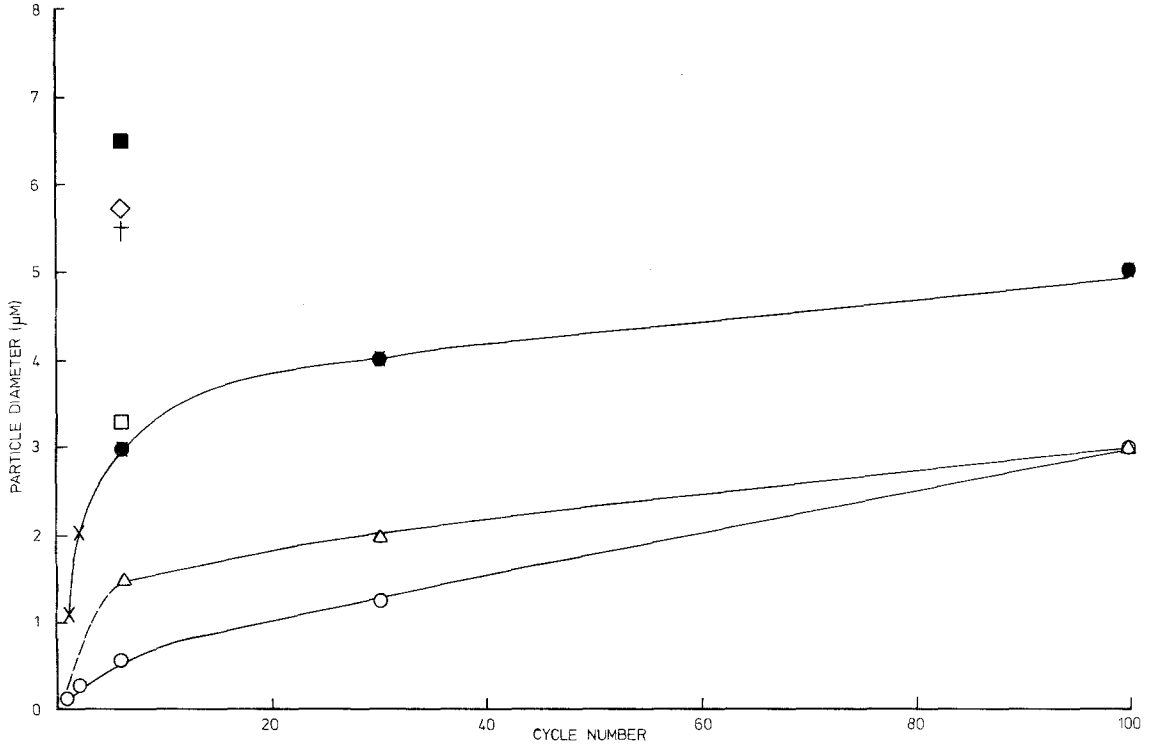

Fig. 33. Particle diameter as a function of cycle number for discharged samples. (i) $C/8$ charge, $C/1$ discharge rates; X, $Cd/Cd(OH)_2$ compacts in electrode edge; ○, trapped Cd in electrode edge; ●, $Cd/Cd(OH)_2$ compacts in electrode interior; △, trapped Cd in electrode interior. (ii) $C/50$ charge, $C/1$ discharge rates; †, $Cd/Cd(OH)_2$ compacts in electrode edge; □, trapped Cd in electrode edge; ■, $Cd/Cd(OH)_2$ compacts in electrode interior; ◇, trapped Cd in electrode interior.

charge may be related to their decreased solubility. Such crystals being composed of insulating β-$Cd(OH)_2$ are also unlikely to charge by a direct solid-state route. This is in direct contrast to the behaviour which might be expected for the passive film which is claimed [16] to have a high electronic conductivity and to charge readily via a solid-state process. It seems likely that the burial of Cd metal by large crystalline $Cd(OH)_2$ deposits also involves soluble species rather than a totally solid-state process. This does not exclude the possibility of passivation being initially caused by the formation of a thin layer of $Cd(OH)_2$ via a solid-state process. Further growth of the $Cd(OH)_2$ crystallites could occur on top of the passivating layer later, by purely chemical processes involving redissolution of nearby finely precipitated $Cd(OH)_2$ and its recrystallization (i.e. crystal ripening). Alternatively, cadmate derived from new Cd sites undergoing active dissolution could provide the necessary supersaturation, with the old passive sites providing nuclei for the growth of larger $Cd(OH)_2$ crystals.

It is not entirely clear whether the Cd metal in the large $Cd(OH)_2$ crystal interior arose in the first instance from surface blockage or by loss of electronic contact with the nickel sinter matrix. Throughout the micrographs, the impression gained is that the trapped Cd in general makes little contact with the sinter particles suggesting loss of contact. In a previous study [4] it was observed that if the first cycle discharge was interrupted prior to failure that a small extra capacity was delivered on restarting the discharge. This might be taken as evidence against loss of contact.

The invariance of the first cycle discharge capacity on rate [1, 4] can be interpreted in terms of the generation of a critical volume of $Cd(OH)_2$ leading to surface blockage possibly with some loss of electrical contact. Provided the initial Cd particle size is small ($\sim 0{\cdot}5\ \mu m$) and an adequate free pore volume is available then the first cycle discharge is largely complete ($\sim 90\%$) [1]. This may be related to the minimum thickness of $Cd(OH)_2$ which must be grown round the Cd particles to cause passiviation [2].

If the electrode is cycled at low charge rates ($C/8$ and $C/50$), where growth of large Cd particles is favoured, evidence of passivation or surface blockage is seen as previously discussed, i.e. Fig. 31. In the case of electrodes cycled at the high $C/1$ rate passivation is not so apparent because of the relatively small Cd particles which remain operative in the interior. Migration of active material towards the electrode edge, cf. Weininger and Breiter [8, 9], is a complicating factor. This has a deleterious effect on electrode performance because of the decreased pore volume per unit mass of active material and in extreme cases there may be total blockage of some pores. This results in a band of active material on the edge of the electrode being made progressively obsolete. During extended cycles the charge and discharge processes become more interdependent and the development of highly crystalline $Cd(OH)_2$ contributes progressively to the fall in cycle efficiency. It must also be noted that at low charge rates the charging efficiency becomes impaired to an even greater extent again because of the development of highly crystalline $Cd(OH)_2$ but in this case the growth of large Cd metal particles is of greater significance. Where high charge rates and low discharge rates (e.g. $C/8$ and $C/50$) are employed then the growth of large $Cd(OH)_2$ crystals even in the early cycles can be considerable and inefficiencies in the charge process may be greater than those on discharge [4, 25].

Acknowledgements

The authors are indebted to Mr M. Oates and Mr V. Sudra for the photographic reproductions and to the Directors of Ever Ready Company (Holdings) Limited for permission to publish.

References

[1] R. Barnard, A. H. Rafinski, J. A. Lee and F. L. Tye 'Power Sources 5', Proc. 9th Int. Power Sources Symp, (Ed. D. H. Collins), Academic Press, London (1975) p. 183.

[2] J. McCallum and A. H. Reed, Technical Report A. F. APL-TR-72-20, AD 743017, Battelle (1972).

[3] R. D. Armstrong, K. Edmondson and J. A. Lee *J. Electroanal chem.* **63** (1975) 287.

[4] R. Barnard, K. Edmondson, J. A. Lee and F. L. Tye *J. Appl. Electrochem.* To be published.

[5] A. J. Salkind and G. W. Bodamer, 'Batteries 2' Proc. 4th Int. Power Sources Symp. (Ed. D. H. Collins), Pergamon Press (1964) p. 55

[6] J. P. Harivel, B. Morignat and J. Migeon, 'Batteries 2' Proc. 4th Int. Power Sources Symp. (Ed. D. H. Collins), Pergamon Press (1964) p. 107.

[7] E. Luksha, D. J. Gordy and C. J. Menard *J. Electrochem. Soc.* **120** (1973) 1447.

[8] M. W. Breiter and J. L. Weininger, 'Power Sources' Proc. 5th Int. Power Sources Symp. (Ed. D. H. Collins), Pergamon Press (1966) p. 269.

[9] E. Lifshin and J. L. Weininger, *Electrochem Tech* 5 (1967) 5.

[10] E. J. Casey and J. B. Vergette, *Electrochim Acta.* **14** (1969) 897.

[11] P. Bro and H. Y. Kang *J. Electrochem Soc.* **117** (1971) 583.

[12] J. S. Dunning, D. N. Bennion and J. Newman *J. Electrochem Soc.* **118** (1971) 1251.

[13] *Idem, ibid*, **120** (1973) 906.

[14] P. Selanger *J. Appl. Electrochem.* 4 (1974) 249, 259, 263.

[15] R. D. Armstrong, A. D. Sperrin, F. L. Tye and G. D. West, *ibid* **2** (1972) 265.

[16] Y. Okinaka, *J. Electrochem Soc.* **117** (1970) 583.

[17] O. R. Pryakin, V. P. Galushko and E. F. Zavgorodnyaya *Electrokhimiya* 9 (1973) 60.

[18] V. P. Galushko, E. F. Zavgorodnyaya, N. V. Podol'skaya and Yu. P. Rodak, *ibid* 8 (1972) 1216.

[19] F. G. Will and H. J. Hess *J. Electrochem Soc.* **1** (1973) 1.

[20] Yu. I Obed'kov and L. A. L'vova *Electrokhimiya* 9 (1973) 1649.

[21] *Idem, ibid* **10** (1974) 359.

[22] K. Appelt, *Electrochim Acta.* **13** (1968) 1727.

[23] R. D. Armstrong and G. D. West, *J. Electroanal Chem.* **30** (1971) 385.

[24] Y. Okinaka and C. M. Whitehurst *J. Electrochem Soc.* **117** (1970) 583.

[25] R. Barnard, Unpublished work.

[26] F. G. Will, 'Power Sources 2', Proc 6th Int Power Sources Symp. (Ed. D. H. Collins) Pergamon Press (1968) p. 149.

[27] R. D. Armstrong and K. Edmondson *J. Electroanal Chem.* **53** (1974) 371.